Dynamic and Thermodynamic Influences of the Tibetan Plateau on the Atmosphere in a General Circulation Model

QINGLIN ZHENG* AND KUO-NAN LIOU

Department of Meteorology, University of Utah, Salt Lake City, UT 84112

(Manuscript received 13 May 1985, in final form 2 January 1986)

ABSTRACT

The dynamic and thermodynamic influences of the Tibetan Plateau on the temperature, geopotential height, horizontal wind, vertical velocity, cloud and precipitation patterns over eastern Asia are physically investigated employing a general circulation model specifically designed for medium range weather prediction. The model is a modification and improvement of the one recently presented by Liou and Zheng. Efficient and accurate numerical techniques have been devised for the computation of the pressure gradient force and the initial field in the vicinity of mountains in the σ-coordinate. In addiiton, a cumulus convection scheme and a liquid water content prediction equation from which the large-scale precipitation may be evaluated have been developed. Utilizing the NMC objective analysis data covering the period from 13 May to 18 May 1979 and in light of the general circulation model experimentation, we find that incorporation of the mountain and the subsequent diabatic heating effects improves the overall modeling results for the temperature, geopotential height, and wind fields, especially in low and middle levels. Without the consideration of the mountain effects, the prediction results from the model in the low level deteriorate and errors propagate into levels aloft. The thermodynamic effects involving radiation, condensation, and the vertical transport of sensible heat are found to be very important in the maintenance of the position and intensity of the eastern Asia jet stream. Moreover, the presence of the orographic barrier strengthens the vertical velocity, and the effects of the facing and lee sides of the plateau on atmospheric flows significantly influence the prediction of temperature and geopotential height fields. Finally, it is observed that the formation of cloud and precipitation distributions east and south of the plateau is a direct consequence of the coupling of dynamic and diabatic heating effects caused by the plateau.

1. Introduction

It has been recognized that the Tibetan Plateau, which covers about 2.4 million square kilometers, with an average height of over 4 km, has a profound influence on the general circulation of the atmosphere due to its dynamic barrier and the subsequent thermodynamic effects. The importance of the Tibetan Plateau as an elevated heat source for the formation and maintenance of the Asian summer monsoon has long been recognized (Staff Members, 1957; Yeh and Gao, 1979; Yeh, 1981; Luo and Yanai, 1983). In particular, it has been suggested that the onset of Meiyü, or the east Asian summer monsoon rainfall period, is related to the sudden shift in the subtropical westerly jet stream from the southern to the northern periphery of the Plateau (Yin, 1949; Kasahara, 1980; Tao and Ding, 1981; Murakami and Ding, 1982). Also, it is believed that the summertime heavy rainfall frequently occurring in central China is produced by vortices which form over the Tibetan Plateau (Tao and Ding, 1981; Zhou and Hu, 1982; Shen et al., 1985a,b).

Based on the available data, a number of analyses have been carried out to understand the heat and moisture sources and sinks over the Plateau region. Reiter and Gao (1982) estimated the heating effects of the Tibetan Plateau which are believed to play an important role in the development and movement of the South Asian anticyclone and in the Indian monsoon development. Murakami and Ding (1982) analyzed the wind and temperature changes over the Tibetan Plateau during the early summer of 1979. They noted that the strong upper jet stream in the westerlies at 300 mb shifts northward from ~30°N to ~35°–40°N on 3–4 June and indicated that the increased temperature over the plateau area may be caused by adiabatic heating. Nitta (1983) computed variations of the heat sources over the eastern Tibetan Plateau using the FGGE II-b upper air data for the summer of 1979. He found a maximum heating of ~4°C day^{-1} over the plateau around 400 mb, which is contributed to almost equally by the sensible and latent heat release. He also found that the heat source over the plateau has a period of longer than 10 days and correlates with the variations of precipitation over central India. Luo and Yanai (1983, 1984) computed the heat and moisture budgets, as well as precipitation over the Tibetan Plateau during a 40-day period in May–June 1979. The regions of the

* Permanent affiliation: Academy of Meteorological Science, State Meteorological Administration, Beijing, China.

sources and sinks of heat and moisture over the plateau and the surrounding areas were illustrated. Chen et al. (1985) estimated the variability of the heat source over Tibet for the summer of 1979, utilizing new surface data which were recently made available and Nimbus-7 satellite data. They indicated that the assumption of the drag coefficient is critical to the estimate of the heat fluxes and heating rates.

Numerous GCM integrations have been carried out to investigate the orographic effects on the large-scale features. Using a six-layer GCM for the simulation of the January climate, Kasahara and Washington (1971) found that the dynamic effect of mountains appeared to be less than their thermodynamic effect and that the inclusion of mountains did not significantly alter the distribution of precipitation. Manabe and Terpstra (1974) performed numerical experiments using a GCM with and without the consideration of the effects of mountains. They concluded that the probability of cyclogenesis increases significantly on the lee side of the mountains and that the mountains greatly affect the global distribution of precipitation. Further, Hahn and Manabe (1975) investigated the role of the Tibetan Plateau in the southern Asia monsoon circulation using an 11-level GCM. They found that the presence of mountains is instrumental in maintaining the southern Asia low pressure system and that much higher temperatures are produced in the middle and upper troposphere over the Tibetan Plateau. The results of GCM simulations reported by Gates (1982) indicated that the Tibetan Plateau influences the southeastern Asia monsoon which, in turn, profoundly affects the regional summer climate. Kuo and Qian (1981) investigated the thermodynamic and dynamic effects of the Tibetan Plateau on the monsoon circulation and the climate of Asia utilizing a simplified circulation model; they illustrated the importance of the thermal effects on the distribution of the geopotential height and temperature fields in the Tibetan region. Kuo and Qian (1982) carried out further numerical experiments to understand the relative importance of radiative heating and deep cumulus convection for the development of the mean monsoon circulation over the region 0°–180°E and 25°S–55°N in July. They found that the surface pressure and flow patterns are primarily determined by the diabatic heating distribution and, to a lesser degree, by orography. However, the precipitation distribution from the model is critically affected by both diabatic heating and orography. Nakamura and Murakami (1983) and Murakami and Nakamura (1983) investigated the effects of the Tibetan Plateau on the mean flow and low-level cold surges using a ten-layer dry numerical model in which Newtonian cooling is employed to account for the thermal effect. They showed, from the hypothetical experiments, that the westerly jet tends to flow around rather than over the mountains and splits into two branches in the lower troposphere, and reported that the computed features are in agreement with those described by Murakami (1981). Moreover, Chen and Dell'Osso (1984) performed numerical experiments using the ECMWF global grid point model to study heavy rainfall in central China which originated from a vortex over the Tibetan Plateau. They showed that the latent heat release played a significant role in the intensity of the upper-level easterlies. More recently, Shen et al. (1985a,b) conducted a number of numerical experiments, employing a six-layer hydrodynamic primitive-equation model, to investigate the effects of the vortices which develop over the Tibetan Plateau during the summer on the severe weather in eastern China. In contrast to Chen and Dell'Osso's findings, they indicated that the vortices over the eastern part of the Plateau are closely related to sensible heating effects.

It is evident, based on the aforementioned GCM and model experiments, that the effects of mountains on the climatic state of the atmosphere is quite important. To the best of our knowledge, however, the dynamic and thermodynamic effects of the mountains, in general, and the Tibetan Plateau, in particular, on the flow pattern and the temperature and precipitation distributions from the point of view of medium range weather prediction have not been comprehensively investigated utilizing a general circulation model.

It is the objective of this paper to explore the influence of the Tibetan Plateau on the large-scale features over eastern Asia from both the dynamic and thermodynamic perspectives, employing the general circulation model reported by Liou and Zheng (1984; hereafter referred to as LZ). As pointed out in that paper, the model is basically designed for short and medium range weather prediction, in which specific attention has been given to the radiation and cloud parameterizations and cloud-radiation interactions. However, in order to examine the dynamic and subsequent thermodynamic effects of mountains on large-scale flow patterns, we have made a number of improvements and modifications to the model described in LZ. Specifically, we have developed accurate and efficient numerical techniques to calculate the pressure gradient force and initial field in the vicinity of mountains in the σ-coordinate, as well as to reduce the transformation error from the σ- to p-coordinates for the prediction result in the σ-coordinate. These numerical techniques are discussed in section 2. In addition, we have incorporated a cumulus convection scheme combining the criteria described by Arakawa (1969) and the average heating rate profile proposed by Kuo (1965, 1974). This is presented in section 3 where we have also described a liquid water content prediction equation from which the large-scale precipitation can be computed. In section 4, we report the dynamic and thermodynamic effects of the Tibetan Plateau on the predicted temperature and geopotential height fields,

as well as on the predicted zonal wind and vertical velocity profiles. Where possible, attempts have been made to isolate the pure dynamics or dynamic–thermodynamic coupling effects on the prediction results in five-day simulation experiments with and without the inclusion of the effects of mountains. Finally, the highlights of the present numerical experiments are summarized in section 5.

2. Model improvement in dynamic aspects

a. The effects of mountains

It is well known that the use of the σ-coordinate system, introduced by Phillips (1957), removes the difficulty in the representation of the lower-boundary conditions in such a manner that the surface pressure follows the terrain height. Unfortunately, in the computation of the pressure gradient force, utilizing the σ-coordinate system in the vicinity of mountains produces another problem associated with the small difference between two large quantities. Although numerous research efforts have attempted to resolve this problem in large-scale numerical modeling, the solution appears to be far from satisfactory at this point. In LZ, the numerical scheme designed for the divergence equation had the specific property of overcoming the problem concerning small differences due to two large values, especially when the expanded wavenumbers were limited (<20) in the computation. In this paper we propose a numerical scheme to deal with the computation of the pressure gradient force in the vicinity of mountains.

To introduce our proposed method, we write the horizontal equations of motion in the forms

$$\frac{\partial u}{\partial t}+\frac{u}{a\sin\theta}\frac{\partial u}{\partial \lambda}+\frac{v}{a}\frac{\partial u}{\partial \theta}+\dot{\sigma}\frac{\partial u}{\partial \sigma}+fv+\frac{uv}{a}\cot\theta = B_\lambda^\phi+F^u+\frac{g}{P_*}\frac{\partial \tau^u}{\partial \sigma}, \quad (2.1)$$

$$\frac{\partial v}{\partial t}+\frac{u}{a\sin\theta}\frac{\partial v}{\partial \lambda}+\frac{v}{a}\frac{\partial v}{\partial \theta}+\dot{\sigma}\frac{\partial v}{\partial \sigma}-fu-\frac{u^2}{a}\cot\theta = B_\theta^\phi+F^v+\frac{g}{P_*}\frac{\partial \tau^v}{\partial \sigma}, \quad (2.2)$$

where the pressure gradient force terms in the u and v components are defined by

$$B_\lambda^\phi=\left(-\frac{1}{a\sin\theta}\frac{\partial \phi}{\partial \lambda}-\frac{RT}{a\sin\theta}\frac{\partial \ln P_*}{\partial \lambda}\right)_\sigma = \left(-\frac{1}{a\sin\theta}\frac{\partial \phi}{\partial \lambda}\right)_p, \quad (2.3)$$

$$B_\theta^\phi=\left(-\frac{1}{a}\frac{\partial \phi}{\partial \theta}-\frac{RT}{a}\frac{\partial \ln P_*}{\partial \theta}\right)_\sigma = \left(-\frac{1}{a}\frac{\partial \phi}{\partial \theta}\right)_p. \quad (2.4)$$

In Eqs. (2.1)–(2.4), θ = 90°-latitude, λ is the longitude, a the radius of the earth, $\sigma = P/P_*$ with P_* the pressure at the surface, f the Coriolis parameter, R the universal constant for air, and g the gravitational acceleration. Also, F^u and F^v denote, respectively, the horizontal eddy nonlinear viscosity terms for the u and v velocity components; τ^u and τ^v are, respectively, the vertical diffusion terms for the u and v components; T the temperature; and ϕ the geopotential height. Finally, the notation $(\ )_\sigma$ or $(\ )_p$ represents, respectively, the terms in the σ- or p-coordinate system. In Eqs. (2.3) and (2.4) we have expressed the pressure gradient force terms in the pressure coordinate system directly. By means of this direct expression, the problem concerning terms with large values in the σ-coordinate system has, in principle, been removed. This has been the conventional approach taken to circumvent the aforementioned shortcoming. (See, e.g., Holloway and Manabe, 1971.) However, to utilize this method, it is necessary to transfer the geopotential height field ϕ on the σ-surface to the isobaric surface at every time step in the computation; in so doing, errors will be generated through numerical interpolations. In addition, the lack of prediction values within the mountainous region will also lead to severe difficulties in the calculation of pressure forces in the neighborhood of the mountain. Moreover, the computational effort will be significantly increased due to this transformation, especially in the spectral model.

For these reasons, we wish to propose an alternative numerical scheme which is specifically developed for the computation of the pressure gradient forces in the σ-coordinate system. We let the geopotential height field at the time step t be expressed by

$$\phi = \phi_{t_0}+(\phi-\phi_{t_0}), \quad (2.5)$$

where ϕ_{t_0} denotes the geopotential height field at the initial time t_0. Substituting Eq. (2.5) into Eqs. (2.3) and (2.4) leads to

$$B_\lambda^\phi=\left[-\frac{1}{a\sin\theta}\frac{\partial \phi_{t_0}}{\partial \lambda}\right]_p+\left[-\frac{1}{a\sin\theta}\frac{\partial}{\partial \lambda}(\phi-\phi_{t_0})\right]_p, \quad (2.6)$$

$$B_\theta^\phi=\left[-\frac{1}{a}\frac{\partial \phi_{t_0}}{\partial \lambda}\right]_p+\left[-\frac{1}{a}\frac{\partial}{\partial \theta}(\phi-\phi_{t_0})\right]_p. \quad (2.7)$$

Next, the first terms on the right-hand side of Eqs. (2.6) and (2.7) remain unchanged; i.e., we employ the initial geopotential height field in the pressure-coordinate throughout the prediction computation. However, we perform the transformation of the second terms on the right-hand side from the pressure-coordinate to the σ-coordinate system to get

$$\left.\begin{aligned} B_\lambda^\phi &= \left[-\frac{1}{a\sin\theta}\frac{\partial\phi_{t_0}}{\partial\lambda}\right]_p \\ &\quad + \left[-\frac{1}{a\sin\theta}\frac{\partial}{\partial\lambda}(\phi-\phi_{t_0}) - \frac{R(T-T_{t_0})}{a\sin\theta}\frac{\partial}{\partial\lambda}\ln P_*\right]_\sigma \\ B_\theta^\phi &= \left[-\frac{1}{a}\frac{\partial\phi_{t_0}}{\partial\theta}\right]_p \\ &\quad + \left[-\frac{1}{a}\frac{\partial}{\partial\theta}(\phi-\phi_{t_0}) - \frac{R(T-T_{t_0})}{a}\frac{\partial}{\partial\theta}\ln P_*\right]_\sigma \end{aligned}\right\}, \tag{2.8}$$

where the terms $(\phi - \phi_{t_0})$ and $(T - T_{t_0})$ represent the deviation of the predicted geopotential height and temperature fields in the σ-coordinate from the initial values. Note that at any time step, $(\phi - \phi_{t_0})$ may be computed from $(T - T_{t_0})$ via the hydrostatic equation. In view of the foregoing analysis, the interpolation of the geopotential height field from σ-surface to the isobaric surface is done only at the initial time step. Also, it is quite evident that the geopotential height and temperature fields that we are dealing with are deviations from their respective initial fields which are normally small values. As such, the problem associated with the small differences between two large quantities produced by pressure force terms in the σ-coordinate system in the vicinity of mountains is largely removed by the efficient computational method presented above.

b. An efficient interactive method for the computation of the initial field in the σ-coordinate

The problem here is concerned with the interpolation and/or extrapolation of the large-scale variables between the σ- and p-surfaces. Let

$$R_{p,t_0} = [\phi, T, u, v, q]_{p,t_0} \tag{2.9}$$

denote the known distributions of the geopotential height, temperature, u and v velocity, and the specific humidity fields at the initial time frame in the pressure-coordinate. Assume that method A (e.g., logarithmic interpolation) is used to get the distribution of the large-scale variables in the σ-surface, defined by

$$R_{\sigma,t_0} = [\phi, T, u, v, q]_{\sigma,t_0}. \tag{2.10}$$

It has been the conventional approach to employ R_{σ,t_0} directly for the model initial field to predict $R_{\sigma,t}$. To get $R_{p,t}$ on the isobaric surface at some time step t for presentation and performance verification, reverse interpolations, which may use method A or a different method, say B, are then carried out.

Because the observed large-scale variables for initialization are available only at a few isobaric surfaces, interpolations to the σ-surface will generally produce significant errors. In order to minimize these errors, we have devised an efficient computational scheme for initialization. We first use method A to get the large-scale variables at the σ-surface from available observed data. We then reverse the interpolation utilizing either method A or B to obtain these variables back to the isobaric surface. Symbolically, we write

$$R_{p,t_0}{}^{(0)} \xrightarrow{\text{A}} R_{\sigma,t_0}{}^{(1)} \xrightarrow{\text{A or B}} R_{p,t_0}{}^{(1)}. \tag{2.11}$$

Let the errors caused by numerical interpolations be denoted by

$$\Delta R_{p,t_0}{}^{(1)} = R_{p,t_0}{}^{(0)} - R_{p,t_0}{}^{(1)}. \tag{2.12}$$

Subsequently, we may perform the same interpolation scheme on the errors in such a manner that

$$\Delta R_{p,t_0}{}^{(1)} \xrightarrow{\text{A}} \Delta R_{\sigma,t_0}{}^{(1)} \xrightarrow{\text{A or B}} \Delta R_{p,t_0}{}^{(2)}. \tag{2.13}$$

It follows that

$$R_{\sigma,t_0}{}^{(2)} = R_{\sigma,t_0}{}^{(1)} + \Delta R_{\sigma,t_0}{}^{(1)}. \tag{2.14}$$

Thus, the procedure may be repeated until such a time that $\Delta R_{\sigma,t_0}{}^{(N)} \to 0$ where N is the total number of iterations. Mathematically, we may then write

$$R_{\sigma,t_0} = R_{\sigma,t_0}{}^{(N+1)} = R_{\sigma,t_0}{}^{(1)} + \sum_{n=0}^{N-1} \Delta R_{\sigma,t_0}{}^{(n+1)}. \tag{2.15}$$

On the basis of a series of numerical experiments, we find that two iterations are sufficient to converge the errors encountered in the interpolation; that is $(N = 2)$,

$$\Delta R_{p,t_0}{}^{(N)} = R_{p,t_0}{}^{(0)} - R_{p,t_0}{}^{(N)} \to 0. \tag{2.16}$$

In Table 1, we list the rms values of $\Delta R_{p,t_0}{}^{(1)}$ and $\Delta R_{p,t_0}{}^{(3)}$ for a number of examples utilized in the experiments. The rms is defined by

$$\epsilon^{(N-1)} = \frac{1}{N}\left\{\sum_{i,j}[\Delta R_{p,t_0}{}^{(N)}(i,j)]^2\right\}^{1/2}. \tag{2.17}$$

As shown in this table, after two iterations, the errors in temperatures and velocities are already in the second decimals.

c. Reduction of the transformation error from σ- to p-coordinates for the predicted result in the σ-coordinate

Let R_{σ,t_N} denote the predicted result in the σ-coordinate and consider the following integration:

$$\left(\int_{t_0}^{t_N}\frac{\partial}{\partial t}R_{\sigma,t}dt\right)_{\sigma\to p} = (R_{\sigma,t_N} - R_{\sigma,t_0})_{\sigma\to p}. \tag{2.18}$$

TABLE 1. Root-mean-square values.

	$\epsilon^{(0)}$	$\epsilon^{(1)}$	$\epsilon^{(2)}$
T (°C)	0.621	0.056	0.018
u (m s^{-1})	1.57	0.223	0.071
v (m s^{-1})	2.11	0.292	0.083

The term on the right may be written

$$(R_{\sigma,t_N} - R_{\sigma,t_0})_{\sigma\to p} = (R_{\sigma,t_N})_{\sigma\to p} - (R_{\sigma,t_0})_{\sigma\to p}. \quad (2.19)$$

Since R_{σ,t_0} is obtained from R_{p,t_0} at the initial time, we should have

$$(R_{\sigma,t_0})_{\sigma\to p} = R_{p,t_0}. \quad (2.20)$$

It follows from Eqs. (2.19) and (2.20) that

$$(R_{\sigma,t_N})_{\sigma\to p} = R_{p,t_0} + (R_{\sigma,t_N} - R_{\sigma,t_0})_{\sigma\to p}. \quad (2.21)$$

In this manner, the transformation is performed with reference to the difference between the predicted results and initial data, which will be much smaller than the predicted results themselves. Also, by utilizing Eq. (2.21), it is guaranteed that the predicted result will be on the same order of magnitude as the initial data. To perform the transformation of the difference from the σ- to p-coordinates, we may follow the procedure described in section 2b to reduce the errors which may be encountered in the computation.

3. Model improvement in thermodynamic aspects

In this section, we wish to describe a cumulus parameterization program and an interactive cloud formation program, including the liquid water content prediction, for incorporation into the general circulation model developed by LZ. We first modify the thermodynamic and water vapor transport equations presented in that paper in the forms:

$$\frac{\partial T}{\partial t} + \frac{u}{a\sin\theta}\frac{\partial T}{\partial \lambda} + \frac{v}{a}\frac{\partial T}{\partial \theta} - \left(\frac{RT}{C_p\sigma} - \frac{\partial T}{\partial \sigma}\right)\dot{\sigma} - \frac{RT}{C_p}\frac{d}{dt}\ln P_* = Q^R + Q^L + F^T + \frac{g}{P_*}\frac{\partial \tau^T}{\partial \sigma}, \quad (3.1)$$

$$\frac{\partial q}{\partial t} + \frac{u}{a\sin\theta}\frac{\partial q}{\partial \lambda} + \frac{v}{a}\frac{\partial q}{\partial \theta} + \dot{\sigma}\frac{\partial q}{\partial \sigma} = q^L + F^q + \frac{g}{P_*}\frac{\partial \tau^q}{\partial \sigma}, \quad (3.2)$$

where Q^L and q^L denote, respectively, the heating rate and water vapor sink due to condensation. All other notations are conventional and defined in LZ.

We postulate that the small-scale cumulus convection and large-scale stable cloud formation are mutually exclusive, physically and statistically, so that Q^L and q^L may be written

$$Q^L = \begin{cases} Q^C, & \text{cumulus convection} \\ Q^{NC}, & \text{stable cloud formation} \end{cases}, \quad (3.3)$$

$$q^L = \begin{cases} q^C, & \text{cumulus convection} \\ q^{NC}, & \text{stable cloud formation} \end{cases}. \quad (3.4)$$

The computation of these terms and the associated precipitation under appropriate atmospheric conditions are described subsequently.

a. Cumulus convection

It has been well known that a significant portion of the large-scale disturbances in the tropics are driven by the latent heat release which takes place primarily in deep cumulus towers. Because the horizontal scale of these cumulus clouds is much smaller than the grid scale utilized in representing the large-scale flows, their activities can only be incorporated into the large-scale equations via parameterization. Pioneering work on the parameterization of cumulus convection has been proposed by Kuo (1965, 1974), Ooyama (1971), Arakawa and Schubert (1974), and Anthes (1977) who modified Kuo's scheme. More recently, the effects of incorporating various cumulus parameterization schemes into general circulation models on the performance of such models have been investigated by Donner et al. (1982) who employed Kuo's scheme and by Albrecht (1983) who utilized a parameterization theory proposed by Arakawa and Schubert.

In connection with our model development, we have designed a cumulus convection parameterization scheme which follows the concept of the averaged heating rate profile proposed by Kuo. However, we have also adopted the criteria described by Arakawa and Schubert for the onset of cumulus convection.

First, in order for the cumulus convection to occur, it is necessary that the buoyancy force be positive so that the virtual temperature in the cloud region $T_{v,c}$ is greater than that in the clear region $T_{v,0}$. In accordance with Arakawa and Schubert, we must have

$$T_{v,c} - T_{v,0} \approx \frac{1}{C_p + L(\partial q_s/\partial T)}(E_c - E_0) > 0, \quad (3.5)$$

where q_s is the saturation water vapor mixing ratio, L the latent heat per unit mass, and E_c and E_0 are the moist static energy for the cloud and clear column under saturation conditions, respectively, with $E = C_pT + \Phi + Lq$. Since $\partial q_s/\partial T > 0$, an alternate criterion for cumulus convection to occur will be to test whether E_c is greater than E_0. According to Arakawa (1969), cumulus convection may be divided into three types: penetrating (A1), low-level (A2), and middle-level (A3) convections. In reference to Fig. 1 in LZ, the criteria may be expressed by

$$\left.\begin{aligned} E_c(\sigma_{13}) &> E_0(\sigma_5) \\ E_c(\sigma_{13}) &< E_0(\sigma_7) \end{aligned}\right\} \quad \text{for A1,} \quad (3.6a)$$

$$\left.\begin{aligned} E_c(\sigma_{13}) &> E_0(\sigma_7) \\ E_c(\sigma_{13}) &< E_0(\sigma_5) \end{aligned}\right\} \quad \text{for A2,} \quad (3.6b)$$

$$E_c(\sigma_7) > E_0(\sigma_5) \quad \text{for A3.} \quad (3.6c)$$

For types A1 and A2, we set the cloud base at $\sigma_b = 910\ \text{mb}/P_*$, while for A3, $\sigma_b = 700\ \text{mb}/P_*$.

Once the criterion for the onset of cumulus convec-

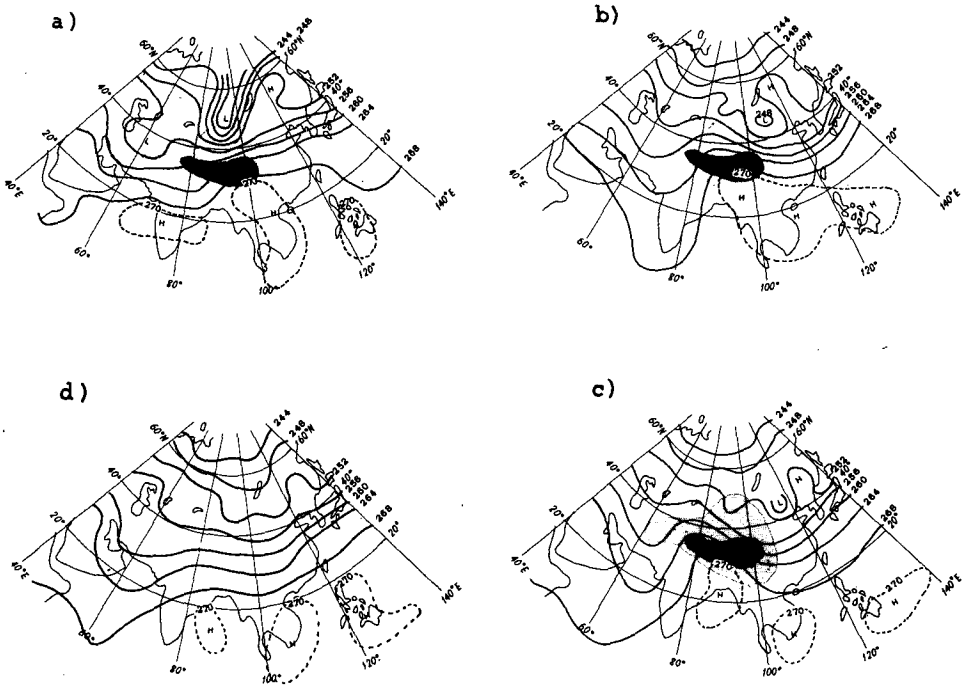

FIG. 1. 500-mb temperature field over eastern Asia (a) for the initial day, 13 May 1979, (b) for the five-day average, 14–18 May 1979, analyzed from observations, (c) for the five-day average, 14–18 May 1979 predicted from the model with the inclusion of mountains, and (d) same as in (c) except without mountains. The contour lines are in units of K.

tion has been met, we then postulate that the latent heat release due to condensation and sublimation must be directly related to the temperature difference between the cloud region and the surrounding air. Thus, we need to find the temperature within the cloud. Since the cloud base has been determined and its temperature is assumed to be the same as that of the ambient air, the cloud temperature may be evaluated by the saturation moist adiabatic processes. In accord with the first law of thermodynamics, the lapse rate in the logarithmic pressure coordinate may be written in the form

$$\frac{\partial \ln T_c}{\partial \ln p} = \beta \frac{1 + Lq_c/(RT_c)}{1 + L^2 q_c/(R_v C_p T_c^2)}, \tag{3.7}$$

where $\beta = R_d/C_{pd} = 0.2856$, $q_c = \tilde{h}_c q_s$ and $\tilde{h}_c$ is the critical relative humidity associated with cumulus convection which is taken to be 0.8. As previously noted, $T_c(z_b) = T(z_b)$. Upward stepwise calculations will then give the cloud temperature at the model layer. Note that we have not considered entrainment in the calculation of the cloud temperature.

In accordance with the parameterization principle proposed by Kuo, the averaged heating rate profile within a grid cell may be expressed by

$$Q^C \propto k_c(T_c - T), \tag{3.8}$$

where the coefficient of proportionality k_c, which in essence is an effective exchange coefficient, is given by Kuo (1974) and Donner et al. (1982) as

$$k_c = (1 - b)M_t g P_*/[(\sigma_b - \sigma_t)\langle T_c - T\rangle], \tag{3.9}$$

with

$$1 - b = \frac{1}{0.6}\int_{\sigma_t}^{\sigma_b} \frac{q}{q_c}\, d\sigma, \tag{3.10}$$

$$M_t = -\frac{P_*}{g}\int_{\sigma_t}^{\sigma_b} (\nabla \cdot \mathbf{V}q)d\sigma + \rho_0 C_D |\mathbf{V}_0|[q_s(1) - q(1)], \tag{3.11}$$

$$\langle T_c - T\rangle = \frac{1}{\sigma_b - \sigma_t}\int_{\sigma_t}^{\sigma_b} (T_c - T)\frac{d\sigma}{g}. \tag{3.12}$$

where ρ_0 is the air density at the surface, $\mathbf{V}_0$ the surface velocity, C_D the drag coefficient and σ_b and σ_t the pressure levels corresponding to the base and top, respectively, of the cumulus cloud. Moreover, it is noted that $q^C \propto k_c(q_c - q)$. The drag coefficient values used in this study are 0.0015 (over the ocean), 0.002 (lower than 800 m over land) and 0.003 (higher than or equal to 800 m over mountains). The importance of the drag coefficient value in connection with the model simulation involving the Tibetan Plateau was pointed out by Chen et al. (1985) and Shen et al. (1985).

b. Large-scale stable cloud formation

In LZ we devised a cloud formation scheme on the basis of an empirical–statistical procedure. We first compute the cloud cover utilizing the following equation

$$\eta = \begin{cases} [(h - h_c)/(1 - h_c)]^2, & h > h_c \\ 0, & h \leqslant h_c \end{cases} \quad (3.13)$$

where the critical relative humidity h_c was derived by empirical means given by

$$h_c(\sigma) = \sum_{n=0}^{3} a_n \sigma^n + \Delta h_c(\hat{\omega})$$

with a_n's the empirical coefficients. We have also considered and incorporated some aspects of cloud microphysics in terms of mean liquid water content through the examination of the cloud location and development, basically for the purpose of radiative transfer calculations. The liquid water content in our previous work was calculated by means of an ad hoc procedure in which observed cloud particle size characteristics for various cloud types were utilized. In this paper, we wish to introduce an interactive liquid water content prediction program in our general circulation model.

By virtue of the water mass conservation principle, the time rate of change of the liquid water mixing ratio l at a given level must be associated with the source via condensation (or sublimation) and the sinks via precipitation P and evaporation E of cloud and precipitation particles to the clear portion of the grid cell concerned. Thus, we may write

$$\frac{\partial l}{\partial t} = -\mathbf{V} \cdot \nabla l + Q^{NC}/L - P - (1 - \eta)E/L \quad (3.14)$$

where the first term on the right denotes the horizontal and vertical advection of the liquid water mixing ratio l and the condensation term given in our previous paper is

$$Q^{NC} = -\frac{F\delta L\hat{\omega}\eta}{C_p a^2} \quad (3.15)$$

where F is the thermodynamic factor, $\hat{\omega}$ the large-scale vertical velocity in the σ-coordinate, η the cloud cover, and $\eta = h_c$ if $\omega < 0$ and $h \geqslant h_c$, $\eta = 0$, otherwise. Also, in Eq. (3.4), $q^{NC} = F\delta\hat{\omega}\eta/a^2$. Here we note that the condensation and advection terms may be obtained from the large-scale variables. However, the precipitation and evaporation at a given level need to be parameterized. In Eq. (3.15) we have ignored the vertical transport resulting from the fall velocity of liquid water and the subgrid diffusion of the liquid water mixing ratio.

In large-scale numerical models, precipitation is generally computed from condensation assuming that all of the condensed water vapor falls instantly. Under this crude approximation, the total precipitation per unit area in a time period may then be estimated by

$$P_{l1}^{*} = \frac{P_*}{g} \int_t^{t+\Delta t} \int_0^1 C_p Q^{NC}/L d\sigma dt. \quad (3.16)$$

However, to the extent that only limited and fortunate cloud populations could produce measurable precipitation at the surface, it would seem that a direct parameterization of precipitation from the liquid water content would be a better physical approach. In modeling the convective cloud, Ogura and Takahashi (1971) proposed that precipitation is directly related to the liquid water content, e.g., $P = c_l l$ where c_l (per unit time) denotes an empirical coefficient representing an averaged relaxation time for cloud particles to become precipitation. More recently, in his pioneering study of cloud modeling, Sundqvist (1978), who followed the idea discussed by Kessler (1969) regarding the rate of auto conversion and parameterization of accretion, proposed that

$$P[\sigma(l)] = C_0 l[1 - e^{-(l/l_r)^2}], \quad (3.17)$$

where C_0 and l_r are empirical coefficients which have values of 10^{-4} s^{-1} and 0.5, respectively, according to Sundqvist. These values physically represent, respectively, the time scale required for cloud droplets to become raindrops and the mean liquid water content in precipitation clouds. The precipitation distribution function denoted in Eq. (3.17) appears to be quite reasonable statistically and perhaps physically. Small values of l will lead to a conversion time scale which is relatively long so that the likelihood of precipitation is small. On the contrary, if $l \geqslant l_r$, it is highly probable that such a cloud will produce significant precipitation.

It is conventional knowledge that evaporation within the cloud is normally very small. However, evaporation of precipitation particles may be quite important. Clearly, it must be related to precipitation itself. Sundqvist (1978) assumed that evaporation at a given level is directly proportional to an integrated precipitation rate at that level. In a recent paper by Sundqvist (1981), however, evaporation at a given level is assumed to be proportional to the square root of the integrated precipitation rate at that level. In connection with the present large-scale modeling effort and in recognition of the simplicity of the parameterization approach, we set

$$E(\sigma) = k_E[1 - q/q_s(T)][\tilde{P}(\sigma)]^{1/2}, \quad (3.18)$$

where the empirical coefficient k_E is taken to be 10^{-3} in SI units and the precipitation rate at the level σ per unit time is defined by

$$\tilde{P}(\sigma) = \frac{P_*}{g} \int_0^{\sigma} C_p P d\sigma'. \quad (3.19)$$

At this point, we have a closed system of equations

involving Eqs. (3.13)–(3.15), (3.17)–(3.19). Thus, numerical computations for the liquid water content may be carried out. In finite difference form, Eq. (3.14) may be written

$$\frac{l^{t+\Delta t} - l^{t-\Delta t}}{2\Delta t} = -(\mathbf{V}\cdot\nabla l)^t + (Q^{NC}/L)^t - [P(l)]^t - [(1-\eta)E(l)/L]^t. \quad (3.20)$$

As shown, all the terms on the right-hand side are evaluated at the time step t. With respect to the initialization of the liquid water content, we used the observed mean values for various stratiform cloud types described in LZ.

Finally, the total precipitation due to cumulus convection or large-scale cloud formation is given by

$$P_{tl} = \begin{cases} \dfrac{P_*}{g}\displaystyle\int_t^{t+\Delta t}\int_{\sigma_t}^{\sigma_b} C_pQ^C/L d\sigma dt, & (3.21a) \\ \dfrac{P_*}{g}\displaystyle\int_t^{t+\Delta t}\int_0^1 \tilde{P}(\sigma)d\sigma dt, & (3.21b) \end{cases}$$

where we note that the total precipitation rate generated by cumulus convection is related to the heating rate profile since the liquid water content within the cumulus is not computed in the model.

4. Simulation results and physical discussions

a. The dynamic and thermodynamic effects of the Tibetan Plateau on the predicted temperature field

In this subsection, we wish to investigate the effect of mountains and the coupled diabatic heating on the predicted temperature field. The case selected for presentation here is 13–18 May 1979. Using the NMC objective analysis data covering this period, Fig. 1a illustrates the initial 500-mb temperature field over eastern Asia on 13 May 1979. On this date, there are several noticeable features, including a pronounced low temperature north of the Tibetan Plateau. South of the plateau are three high temperatures extending from the Indian subcontinent to the western Pacific.

In the next five days, the 500-mb temperature patterns change significantly due to the effect of the Tibetan Plateau. In order to include the result for each day in a compact manner, we carried out five-day averages for the observed data as well as for the predicted temperature fields. Shown in Fig. 1b is the observed 500-mb temperature field averaged over a consecutive five-day period. First, it is noted that the plateau is controlled by a relatively strong temperature ridge so that the temperatures in the surrounding area increase significantly during the five-day period. The cold air presiding over the northern Plateau, denoted in the initial field, moved southeastward and weakened. The warm air located over southern India moved northeastward and merged with the highs in southern China. Because of the temperature ridge presiding over the plateau, an impressive cold temperature trough developed west of the plateau and extended to the southern tip of the Indian subcontinent.

Figure 1c depicts the corresponding predicted temperature field from the general circulation model with the inclusion of the mountains and the subsequent diabatic heating effects. As shown, there is general agreement between the predicted and observed fields. In particular, the model correctly predicts the low temperature northeast of the Tibetan Plateau as well as the temperature ridge over the plateau region. The deep temperature trough southwest of the plateau illustrated in the observed field is also predicted from the model although the intensity of the trough is somewhat reduced. Further, the model correctly reproduced the high temperature southeast of the plateau. In order to investigate whether these features are generated through the mountain and subsequent heating effects, we carried out an additional experiment, removing the mountain and heating terms in the thermodynamic equation. This is illustrated in Fig. 1d. The most noted differences are the disappearance of the temperature ridge over the plateau areas and a significant weakening of the northeastern low temperature. It is quite evident that the coupling effects of dynamics and thermodynamics due to the plateau strengthen the formation of the temperature ridge over the region and deepen the trough over the eastern portion of the plateau. As a result, the warm air from the south moves to the mountain region. It is clear from Fig. 1c, d that the effects of mountains and subsequent sensible and latent heating increase the temperature on the order of 2°–4°C over the plateau regions. Since the sensible and latent heating calculations were coupled in the model, we were unable to estimate the individual contributions to the temperature increase in this case. On the other hand, a temperature reduction in the eastern part of China is caused by the forcing of cold air southeastward by the plateau.

b. The dynamic effect of the Tibetan Plateau on the predicted geopotential height field

In this subsection, we investigate the dynamic effects of the Tibetan Plateau on the circulation pattern in eastern Asia. On 13 May 1979, the initial date, eastern Asia is occupied by an intense pressure trough directly north of the Tibetan Plateau (Fig. 2a). This trough extends to the northern part of the Indian subcontinent. The southern part of India and the Bay of Bengal are controlled by a low pressure system. Two subtropical highs, on the other hand, preside over Indochina and the western Pacific.

During the next five days, the low pressure system persists over the Indian subcontinent, as clearly shown

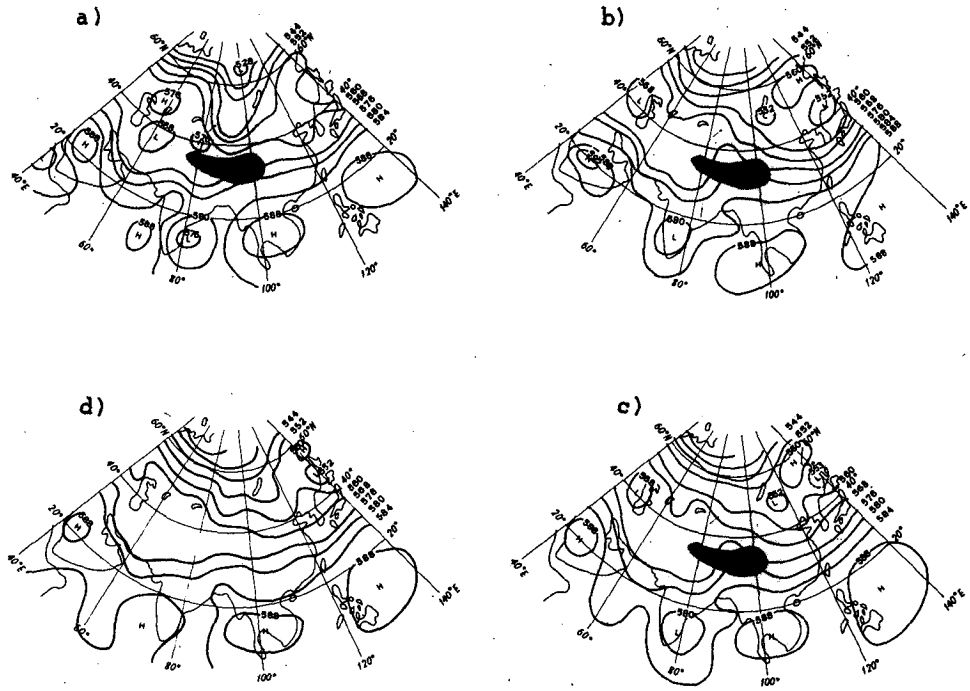

FIG. 2. 500-mb geopotential height field over eastern Asia (a) for the initial day, 13 May 1979, (b) for the five-day average, 14–18 May 1979, analyzed from observations, (c) for the five-day average 14–18 May 1979 predicted from the model with the inclusion of the mountain effect but the diabatic heating term was removed in the experiment, and (d) as in (c) except without mountains.

in Fig. 2b which depicts the five-day averages of the observed 500-mb height field, whereas the trough presiding over the Tibetan Plateau moves eastward and weakens. In fact, a pressure ridge has been established on the plateau. As will be discussed henceforth, both features are produced by the dynamic effect of the plateau.

Figure 2c shows the geopotential height field simulated from the general circulation model with the inclusion of the mountain effects. The diabatic heating term in the thermodynamic equation, however, was removed in the experiment. The low pressure system on the Indian subcontinent and the ridge over the plateau, as well as the subtropical highs are reasonably reproduced. This particular experiment appears to indicate that the dynamic factors associated with mountains are very important for the prediction of the large-scale pressure system.

The flow pattern, after the removal of the Plateau effects, is illustrated in Fig. 2d. The disappearance of the Indian low pressure center and the plateau ridge is quite apparent. We offer the following explanations: First, the forced flow in the lower levels southeastward due to the presence of the Tibetan Plateau, as well as the cyclonic vorticity, assist in the maintenance of the low pressure system. Second, the split flow northeastward tends to intensify the pressure ridge and thereby reduces the existing pressure trough. In addition, the upslope flow in the upper level due to mountain forcing leads to divergence which, in turn, suppresses the cyclonic vorticity. This particular example shows the dynamic effect of the plateau on the general circulation in eastern Asia and the western Pacific and on the monsoon circulation over the Indian subcontinent.

c. *Effects of the Tibetan Plateau on the zonal wind profile*

In this subsection we will consider the dynamic and thermodynamic effects of the Tibetan Plateau on the zonal wind profile over eastern Asia. For this purpose, we present the predicted zonal wind profile on the fourth day, 17 May 1979 (the initial day being 13 May). The profile depicted in Fig. 3a was obtained by averaging the observed zonal winds for longitudes from 50° to 120°E. There are three distinct jets located at approximately 300 mb. The jet at 35°N has velocities exceeding 40 m sec^{-1}. Distinct east winds near the equatorial regions are seen at heights above 300 mb. Near the surface of the plateau, weak east winds are observed. These observed features are well reproduced from the present general circulation model with the inclusion of the effects of mountains, as is evident in Fig. 3b. When the plateau is removed from the model (Fig. 3c), the strong jet located at 35°N is shown to be weakened and shifts southward to about 30°N. The

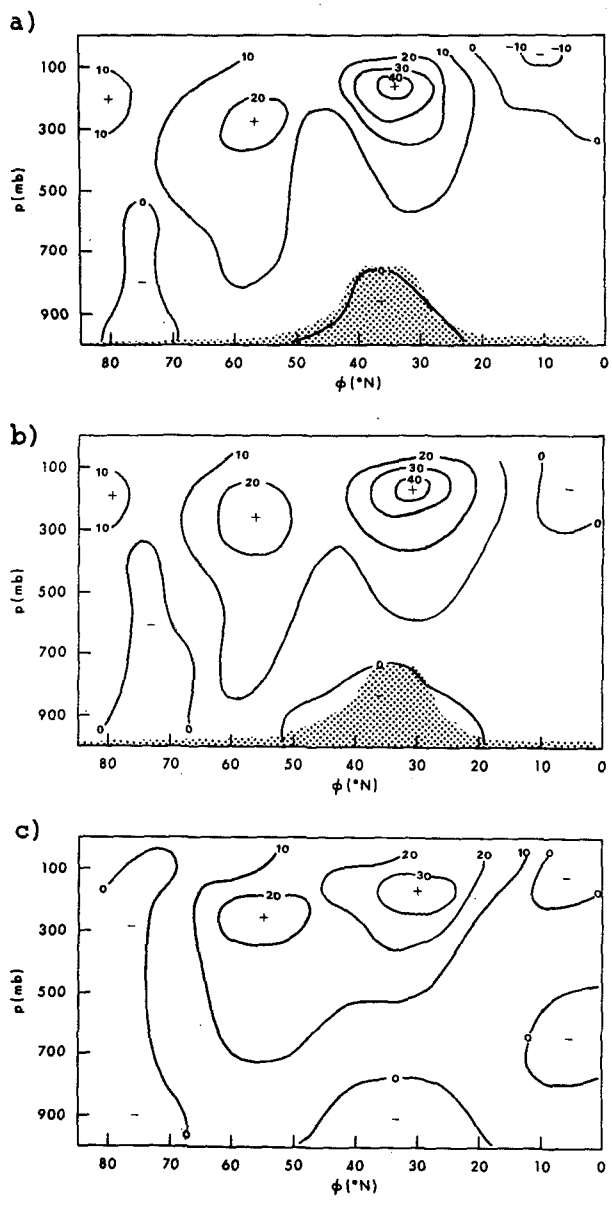

FIG. 3. The averaged zonal wind profile (m sec^{-1}) for longitudes from 50° to 120°E for the fourth prediction day (a) analyzed from observations, (b) predicted from the model with the incorporation of the mountain effects, and (c) as in (b) except without mountains.

difference between the intensity and position of the jet stream is closely associated with the thermodynamic effects caused by the Tibetan Plateau for the following reason: An examination of Fig. 1d shows that temperatures over the plateau are higher than those depicted in Fig. 1c by about 4°C for a five-day average. Thus, the increased (decreased) thermal winds over the northern (southern) plateau region will strengthen (weaken) the west wind. In addition, without the mountain the weak polar jet disappears. Also, it is noted that the easterly wind located at 850–500 mb in the equatorial area is produced by the intensification of the subtropical highs when the effects of the Tibetan Plateau are suppressed in the model.

d. Effects of the Tibetan Plateau on the vertical velocity

To study the effects of the Tibetan Plateau on the vertical velocity, we present the predicted profile along the east–west plane for a fixed latitude of 35°N for the second and fourth days with and without the inclusion of mountains in the general circulation experiments. Figure 4a, b and Fig. 4c, d depict, respectively, the vertical velocity profiles with and without the incorporation of the Tibetan Plateau. First, comparing Fig. 4a, c reveals that the vertical circulations in the vicinity of the Tibetan Plateau increase significantly. On the west side, the upward vertical velocity reaches a maximum value of 22 (in units of 0.5×10^{-4}) mb sec^{-1} near 500 mb. On the lee side, two distinct downward velocity maxima located at about 300 and 600 mb are observed; the lower maximum has a stronger downward velocity than that of the upper one. Thus, the air column stretches vertically so that horizontal convergence takes place between 300 and 600 mb, leading to a greater possibility of cyclonic activity. This is evidenced in the development of the geopotential heights and temperature troughs shown in Figs. 3c and 4c, respectively. On the fourth day, the pattern of vertical velocity profiles is very similar to that on the second day. However, it is seen that the system moves westward so that the upward velocity area extends to the top portion of the mountain. Also, the upward and downward velocity profiles weaken somewhat. In particular, the maximum downward velocity located at 600 mb shifts to 700 mb and weakens by almost a factor of 2. The consequence of the vertical stretch of the air column is especially evident in this case. Figure 4d depicts the predicted vertical velocity for the fourth day without the inclusion of mountains. The aforementioned characteristics, associated with the influence of the Tibetan Plateau, disappear.

e. Effects of the Tibetan Plateau on predicted cloud cover and precipitation

Figure 5a shows the IR cloud picture from the NOAA polar orbiting satellite (available from the Environmental Satellite Imagery, NOAA) for eastern Asia on 18 May 1979 (the fifth day) for verification of the predicted cloud cover with (Fig. 5b) and without (Fig. 5c) the inclusion of mountains. The shaded areas in Fig. 5b, c denote the cloud cover contours greater than 30%. On this date, large-scale cloud systems associated with frontal activities extend from the western Pacific to the Indochina subcontinent. Cloud activity is also evident in the northeastern part of China and the Ko-

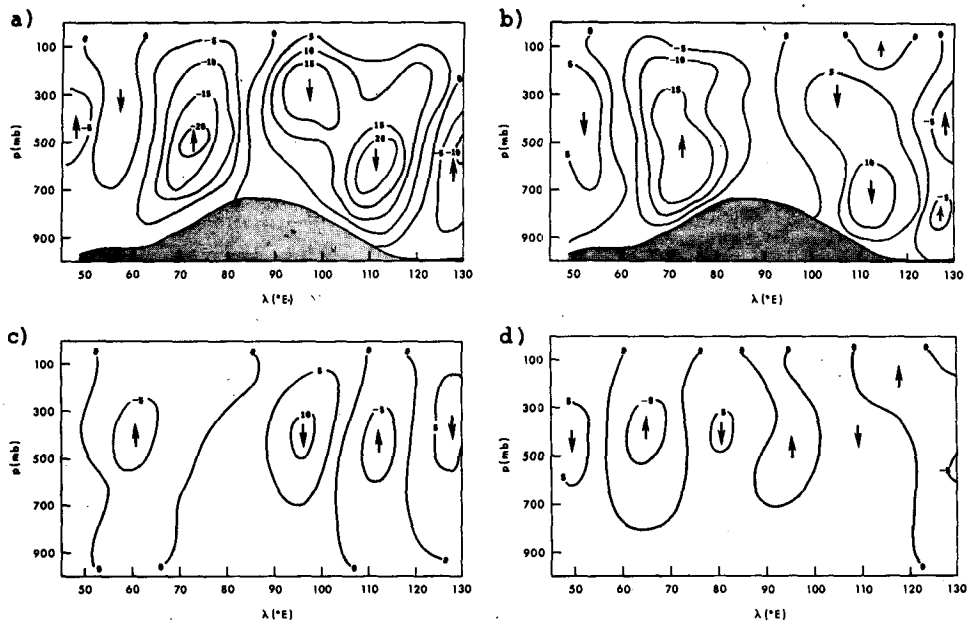

FIG. 4. The predicted vertical velocity profile for a fixed latitude of 35°N (a) for the second day with mountains, (b) for the fourth day with mountains, (c) for the second day without mountains, and (d) for the fourth day without mountains. The contour lines are in units of 0.5×10^{-4} mb sec^{-1}.

rean Peninsula, Tibetan Plateau, and in the vicinity of the Caspian Sea. These cloudy regions, as well as the clear area denoted in the eastern part of China, are generally reproduced from the present model with the inclusion of the mountain effects. When the mountains are removed from the model, the predicted cloud cover is greatly reduced over the Tibetan Plateau and surrounding areas. In addition, the large-scale frontal clouds and the clear portion over the eastern part of China are not correctly reproduced. The physical reason for the improvement of cloud prediction with the incorporation of mountains is quite evident. First, from the foregoing presentation associated with the vertical velocity profile, we find that removing the mountains reduces the upward and downward vertical velocities in the vicinity of the mountains. As a result, the possibility of cloud formation is greatly reduced. Moreover, the presence of the Tibetan Plateau affects the large-scale geopotential height and temperature fields, as illustrated in the preceding figures and, in turn, influences the predicted large-scale cloud field.

In our present model we have incorporated a cumulus parameterization scheme from which precipitation can be evaluated. In addition, we have also modified our large-scale cloud formation method to include the prediction of the liquid water content and the subsequent large-scale precipitation computation. As is well known, the precipitation event is normally associated with meso- or local-scale activity. Therefore, it is difficult to make a direct comparison between the observed data and the predicted values, which are estimated from the model-resolvable parameters. Nevertheless, we have analyzed the total precipitation for the five-day period over some parts of eastern Asia based on the data made available to us from the State Meteorological Administration, People's Republic of China. In Fig. 6b, c we illustrate the predicted precipitation distribution with and without the inclusion of the mountain effects for the five-day prediction experiment. The observed precipitation result is depicted in Fig. 6a where contour lines are plotted from the individual observed values without applying specific smoothing parameters. Based on a combination of rain gage and satellite observations, Krishnamurti et al. (1983) presented daily precipitation for the period 1 May through 31 July 1979. The 24-hour rainfalls were averaged over a 1° latitude/longitude grid. Since we compare the total precipitation for a five-day period, their results will be cross-checked with the present analysis.

Based on the observed data, there are three precipitation maxima centered in northeastern China, Taiwan, and the eastern and southern edges of the Tibetan Plateau. The last center was well illustrated in the daily precipitation maps for the period 14–16 May produced by Krishnamurti et al. The first maximum north of the Gulf of Chihli has a total precipitation of more than 60 mm. Krishnamurti et al. presented a rainfall maximum in this region on 15 May 1979. The predicted precipitation patterns agree with the observed values close to Taiwan and the eastern Tibetan Plateau regions as shown in Fig. 6b. While the precipitation

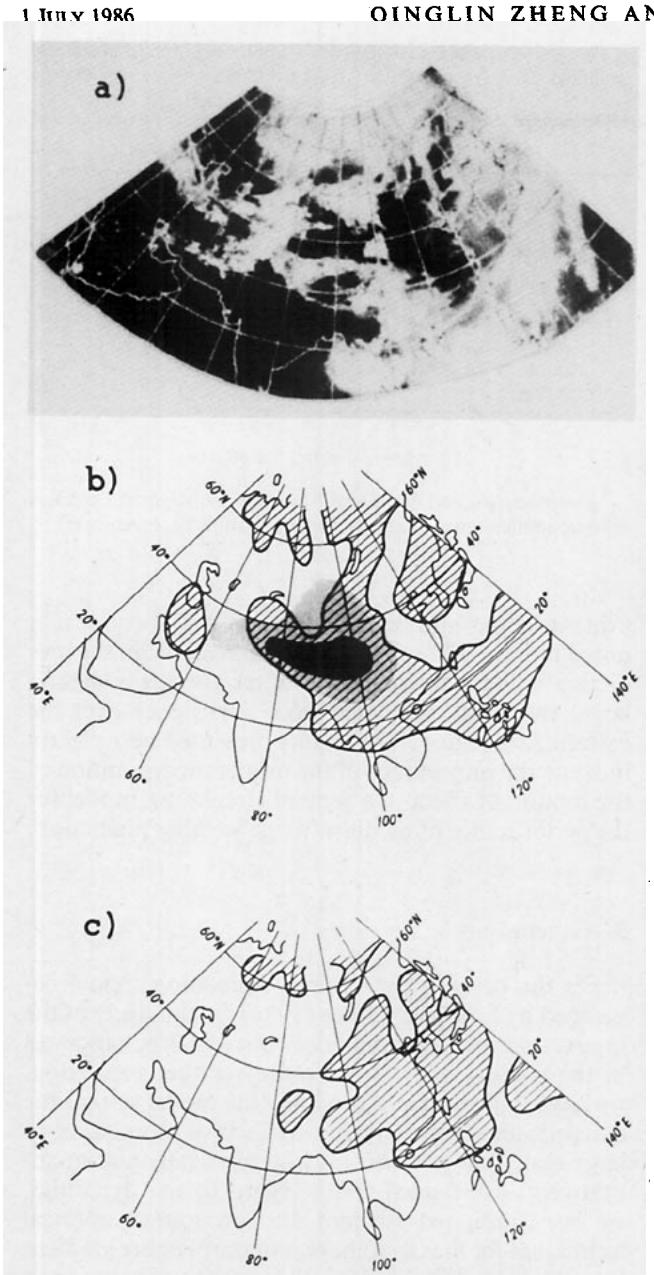

FIG. 5. Cloud cover over eastern Asia on the fifth day, 18 May 1979: (a) observed satellite IR cloud picture; (b) predicted from the model with the mountain effect accounted for; and (c) as in (b) except without mountain effect. In (b) and (c) the shaded areas represent cloud cover greater than 0.3 computed from the model.

area reported over northeastern China is correctly predicted, the model fails to generate the heavy precipitation maximum (~60 mm) probably produced by intensive thunderstorm activities. It is most interesting to note that the model generates reasonable precipitation values on the lee side of the Tibetan Plateau. The maximum computed from the model is primarily associated with the large-scale cloud processes that take place over the southeastern portion of the plateau, and related to the moist southwestern flow from the Gulf of Bengal. Without the incorporation of the mountains in the experiment, the predicted precipitation patterns deviate greatly from the observed data (Fig. 6c). This example illustrates the importance of the coupling of the mountain effects and the subsequent cloud activities to the precipitation prediction.

f. An examination of the dynamic and thermodynamic effects of the Tibetan Plateau on the predicted temperature and geopotential height fields

Finally, we examine the correlation coefficient between the observed and predicted 500-mb temperature and geopotential height changes for a five-day period. The cases studied are with and without the inclusion of the mountain effects and diabatic heatings which include radiative, condensation or cumulus convective, and vertical sensible heat transport sources. The objective of this presentation is to investigate the relative contribution of dynamics (mountains) and thermodynamics (diabatic heatings) to the predicted temperature and height fields.

In Table 2 are listed the correlation coefficients between the observed and predicted 500-mb temperature changes over the region 5°–75°N, 50°–120°E. There are 225 total grid points used in the statistical analysis. It is quite clear that the best temperature prediction performance occurs when both the effects of mountains and diabatic heatings are accounted for in the model; the average temperature correlation coefficient for a five-day period is 81%. However, when neither the contribution of mountains nor the contribution of diabatic heatings is incorporated in the model, the averaged correlation coefficient reduces to 75%. Thus, the contribution of the dynamic and thermodynamic effects lead to an increase in the average correlation coefficient of 6%. When the mountain effect is properly taken into account, the diabatic heatings contribute a 2% increase in terms of the temperature correlation coefficient. The insertion of mountains improves the average temperature prediction by 4% under the condition that no diabatic heatings are accounted for. Finally, without the mountain effect, the incorporation of the diabatic heating terms only contributes to a 1% improvement in the temperature prediction. For the rms errors, all of the predicted results are much smaller than the persistence value. The separation of the mountain and diabatic effects indicates that each contributes almost equally to the temperature prediction.

Table 3a illustrates the correlation coefficients between the observed and predicted 500-mb geopotential height changes and the rms values over the region 15°–55°N, 60°–120°E with 117 total grid point values employed in the statistical analysis. Since the geopotential height field is basically controlled by the dynamic factor via the mountain barrier, only two cases are presented

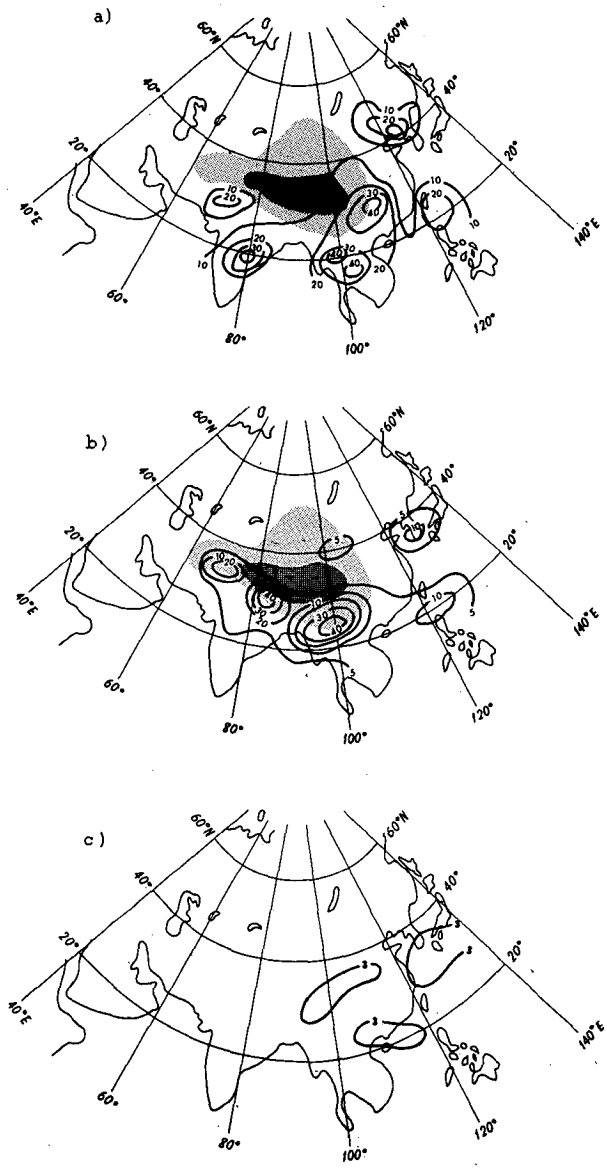

FIG. 6. Total precipitation contour lines in units of mm over eastern Asia for the five-day period, 14–18 May 1979 (a) analyzed from observations, (b) predicted from the model with mountains, and (c) as in (b) except without mountains.

in the table. The average correlation coefficient increases by 5% with the incorporation of the mountain effect and the subsequent diabatic heating. The average predicted rms error is reduced by 5 m when the mountain effect is considered. In comparison with persistence with a value of 82 m, both of the predicted rms errors are much improved. Table 3b lists the predicted rms errors for the fourth day for a number of pressure levels. First, it is clear that the incorporation of the mountains and the subsequent heating effect reduces the predicted rms of the geopotential height field. This is especially

TABLE 2. Correlation coefficient r (%) between the observed and predicted 500-mb temperature changes and the rms over the region, 5–75°N, 50–120°E, for a number of cases studied.†

Case	$\bar{r}$ (%)*	$\overline{\text{rms}}$ (K)*
Persistence	—	4.60
a Yes		
b Yes	81	2.76
a No		
b No	75	3.13
a Yes		
b No	79	2.92
a No		
b Yes	76	3.07

* $\overline{(\ )} = \sum_{i=1}^{5} (\ )_i/5$, where i denotes the day.

† *a* = mountain and *b* = diabatic heating (radiation plus condensation/cumulus convection plus vertical sensible heat transport).

evident at the middle and lower levels. Second, it is noted that the 970-mb rms result derived from the prediction without the inclusion of mountains is slightly larger than that calculated from persistence over the eastern Asia region. The results presented here clearly indicate the importance of the proper incorporation of the mountain effect in a general circulation model for the performance of medium-range weather prediction.

5. Conclusions

On the basis of the general circulation model developed by Liou and Zheng (1984) for the study of the interactions of cloud-radiation and dynamic processes in the context of medium range weather prediction, we have improved and modified the model so that the dynamic and thermodynamic effects of mountains on large-scale flow patterns may be physically and quantitatively investigated. With regard to the dynamics, we have designed efficient and accurate numerical techniques for the computation of the pressure gradient force and the initial field in the vicinity of mountains in the σ-coordinate. With respect to the thermodynamic aspect, we have incorporated a cumulus convection scheme and developed a liquid water content

TABLE 3a. Correlation coefficient r between the observed and predicted 500-mb geopotential height changes on the rms over the region, 15°–55°N, 60°–120°E, for a number of cases studied.

Case	$\bar{r}$ (%)	$\overline{\text{rms}}$ (m)
Persistence	—	82
a Yes		
b Yes	85	47
a No		
b No	80	52

TABLE 3b. The rms (m) of the geopotential height field for the fourth day for a number of pressure levels.

Case	Level (mb) 200	300	500	970
Persistence	121	134	86	66
a Yes *b* Yes	92	80	46	43
a No *b* No	93	84	52	72

prediction equation from which the large-scale precipitation may be evaluated. Utilizing the NMC objective analysis data covering the period from 13 May to 18 May 1979, and employing the present general circulation model specifically designed for medium-range weather prediction, we have investigated the effects of the Tibetan Plateau on the dynamics and thermodynamics of the atmosphere over eastern Asia. Highlights and specific findings of the present numerical experiment are summarized:

1) The predicted 500-mb temperature, geopotential height, and wind fields, as well as the overall prediction results for temperature, geopotential height, and winds within five days are much improved when the mountain effects are properly accounted for in the circulation experiment. The overall prediction results are improved, especially at middle and lower levels, as is demonstrated in subsection 4f.

2) By virtue of the five-day prediction experiments, with and without the inclusion of the mountain and/or diabatic heating effects, we find that the predicted temperature, geopotential height, and wind fields are most reliable when both the mountain and diabatic heating effects are considered. It is suggested that the thermodynamic heating effects are very significant in the maintenance of the jet over eastern Asia in terms of its position and intensity. Based on the present modeling experiment, the consideration of the thermodynamic effects must be coupled with their dynamic counterparts, which are produced by the Tibetan Plateau for the prediction study over eastern Asia. This is due to the fact that without the inclusion of the mountains, the diabatic heating, including radiation, condensation/cumulus convection, and the vertical sensible heat transport, cannot be properly and correctly accounted for in the general circulation model.

3) With respect to the modeling of the vertical velocity, it is observed that the upward and downward components on the west and lee sides of the plateau, respectively, increase significantly in the presence of the plateau. The effects of the west and lee sides of the mountains on atmospheric flows assist in the formation of the ridge over the mountains and in the deepening of the trough east of the mountains. The incorporation of these mechanisms in the five-day experiment evidently leads to a reliable large-scale flow prediction.

4) The presence of the Tibetan Plateau assists in the transfer of the negative vorticity to the northern portion of the Caspian Sea, on the one hand, and continuously strengthens the transfer of the positive vorticity to the southern part of the plateau, on the other. These transfers cause the deepening of the trough south of the plateau, as is apparent in Fig. 2c. On the basis of the present experiment, the maintenance of the low pressure system presiding over the Indian subcontinent appears to be directly related to the mountain effect.

5) The cloud and precipitation distributions over eastern Asia are governed by the dynamic and subsequent thermodynamic heating effects produced by the Tibetan Plateau. Without taking into account the mountain effects, one finds it not possible to reproduce the observed cloud and precipitation patterns, as demonstrated in the present five-day prediction experiment.

In light of the present numerical experiment and on the basis of the present model, it would seem that the extended prediction over a period of ten days to a month may be carried out to investigate the influence of the Tibetan Plateau on the seasonal variations over eastern Asia. The interactions and feedbacks due to the surface heating, cloud-radiation, and dynamic processes caused by the plateau, and their relevance and importance to the large-scale flow and synoptic temperature and prediction patterns may then be examined physically and quantitatively during seasonal variations. Specifically, the mechanisms for the onset of Meiyü, believed to be related to the northward shift of the jet stream south of the Tibetan Plateau, may be investigated physically and dynamically from the modeling point of view.

Acknowledgments. This research was supported in part by the Air Force Geophysics Laboratory under Contract F19628-84-K-004 and by the Division of the Atmospheric Sciences, National Science Foundation, under Grant ATM-81-09050. All of the computations reported in this paper were carried out on the CRAY-1 computer in the National Center for Atmospheric Research, which is supported by the National Science Foundation. Sharon Bennett typed and edited several versions of the manuscript.

REFERENCES

Albrecht, B. A., 1983: A cumulus parameterization for climate studies of the tropical atmosphere. Part I: Model formulation and sensitivity tests. *J. Atmos. Sci.*, **40**, 2166–2182.

Anthes, R. A., 1977: A cumulus parameterization scheme utilizing a one-dimensional cloud model. *Mon. Wea. Rev.*, **105**, 270–286.

Arakawa, A., 1969: Parameterization of cumulus convection. *Proc. WMO/IUGG Symposium on Numerical Weather Prediction*, Tokyo.

——, and W. Schubert, 1974: Interaction of a cumulus cloud en-

semble with the large-scale environment, 1. *J. Atmos. Sci.*, **31**, 674–701.

Chen, L., E. R. Reiter and Z. Feng, 1985: The atmospheric heat source over the Tibetan Plateau from May to August, 1979. *Mon. Wea. Rev.*, **113**, 1771–1790.

Chen, S.-J., and L. Dell'Osso, 1984: Numerical prediction of the heavy rainfall vortex over eastern Asia monsoon region. *J. Meteor. Soc. Japan*, **62**, 730–747.

Donner, L. J., H. L. Kuo and E. J. Pitcher, 1982: The significance of thermodynamic forcing by cumulus convection in a general circulation model. *J. Atmos. Sci.*, **29**, 2159–2181.

Gates, W. L., 1982: The effects of mountains on the atmospheric general circulation and climate. *Proc. of the First Sino-American Workshop on Mountain Meteorology*, Reiter, Zhu and Qian, Eds., Science Press, Beijing, 135–173.

Hahn, D. G., and S. Manabe, 1975: The role of mountains in the South Asian monsoon circulation. *J. Atmos. Sci.*, **32**, 1515–1541.

Holloway, J. L., Jr., and S. Manabe, 1971: Simulation of climate by a global general circulation model. *Mon. Wea. Rev.*, **99**, 335–370.

Kasahara, A., 1980: Influence of orography on the atmospheric general circulation. *Orographic Effects in Planetary Flows*, GARP Publication Series, No. 23, WMO, Geneva, 1–49.

——, and W. M. Washington, 1971: General circulation experiments with a six-layer NCAR model, including orography, cloudiness and surface temperature calculations. *J. Atmos. Sci.*, **28**, 657–701.

Kessler, E., 1969: On the distribution and continuity of water substance in atmospheric circulation. *Meteorological Monographs*, **10**, No. 32, Amer. Meteor Soc., 84 pp.

Krishnamurti, T. N., S. Cocke, R. Pasch and S. Low-Nam, 1983: Precipitation estimates from rain gauge and satellite observations, summer MONEX. Dept. of Meteorology, Florida State University, FSU Report No. 83-7.

Kuo, H. L., 1965: On formation and intensification of tropical cyclones through latent heat release by cumulus convection. *J. Atmos. Sci.*, **22**, 40–63.

——, 1974: Further studies of the parameterization of the influence of cumulus convection on large-scale flow. *J. Atmos. Sci.*, **31**, 1232–1240.

——, and Y. F. Qian, 1981: Influence of the Tibetan Plateau on cumulative and diurnal changes of weather and climate in summer. *Mon. Wea. Rev.*, **109**, 2337–2356.

——, and ——, 1982: Numerical solution of the development of mean monsoon circulation in July. *Mon. Wea. Rev.*, **110**, 1879–1897.

Liou, K. N., and Q. Zheng, 1984: A numerical experiment on the interactions of radiation, clouds and dynamic processes in a general circulation model. *J. Atmos. Sci.*, **41**, 1513–1535.

Luo, H., and M. Yanai, 1983: The large-scale circulation and heat sources over the Tibetan Plateau and surrounding areas during the early summer of 1979. Part I. Precipitation and kinematic analyses. *Mon. Wea. Rev.*, **111**, 922–944.

——, and ——, 1984: The large-scale circulation and heat sources over the Tibetan Plateau and surrounding areas during the early summer of 1979. Part II. Heat and moisture budgets. *Mon. Wea. Rev.*, **112**, 966–989.

Manabe, S., and T. B. Terpstra, 1974: The effects of mountains on the general circulation of the atmosphere as identified by numerical experiments. *J. Atmos. Sci.*, **31**, 3–42.

Murakami, T., 1981: Orographic influence of the Tibetan Plateau on the Asiatic winter monsoon circulation. Part I. Large-scale aspects. *J. Meteor. Soc. Japan*, **59**, 40–65.

——, and Y.-H. Ding, 1982: Wind and temperature changes over Eurasia during the early summer of 1979. *J. Meteor. Soc. Japan*, **60**, 183–196.

——, and H. Nakamura, 1983: Orographic effects on cold surges and lee-cyclogenesis as revealed by a numerical experiment. Part II. Transient aspects. *J. Meteor. Soc. Japan*, **61**, 547–567.

——, and ——, 1983: Orographic effects on cold surges and lee-cyclogenesis as revealed by a numerical experiment. Part I. Time mean aspects. *J. Meteor. Soc. Japan*, **61**, 524–546.

Nitta, T., 1983: Observational study of heat sources over the eastern Tibetan Plateau during the summer monsoon. *J. Meteor. Soc. Japan*, **61**, 590–605.

Ogura, Y., and T. Takahashi, 1971: Numerical simulation of the life cycle of a thunderstorm cell. *Mon. Wea. Rev.*, **99**, 895–911.

Ooyama, K., 1971: A theory of parameterization of cumulus convection. The Syono Memorial Volume. *J. Meteor. Soc. Japan*, **49**, 744–756.

Phillips, N. A., 1957: A coordinate system having some special advantages for numerical forecasting. *J. Meteor.*, **14**, 184–185.

Reiter, E. R., and D.-Y. Gao, 1982: Heating of the Tibetan Plateau and movements of the south Asian high during spring. *Mon. Wea. Rev.*, **110**, 1694–1711.

Shen, R., E. R. Reiter and J. F. Bresch, 1985a: Numerical simulation of the development of vortices over the Qinghai-Xizang (Tibet) Plateau. *Archives Meteor. Geophys. Bioclim.* (accepted).

——, —— and ——, 1985b: Some aspects of the effects of sensible heating on the development of summer weather systems over the Tibetan Plateau. *J. Atmos. Sci.* (submitted).

Staff Members of the Section of Synoptic and Dynamic Meteorology, Inst. of Geophys. and Meteor., Acad. Sin., 1957: On the general circulation over eastern Asia. I. *Tellus*, **9**, 432–446.

Sundqvist, H., 1978: A parameterization scheme for non-convective condensation including prediction of cloud water content. *Quart. J. Roy. Meteor. Soc.*, **104**, 677–690.

——, 1981: Prediction of stratiform clouds: Results from a 5-day forecast with a global model. *Tellus*, **33**, 242–253.

Tao, S.-Y., and Y.-H. Ding, 1981: Observational evidence of the influence of the Qinghai-Xizang (Tibet) Plateau on the occurrence of heavy rain and severe convective storms in China. *Bull. Amer. Meteor. Soc.*, **62**, 23–30.

Yeh, T. C. (Ye, D.), 1981: Some characteristics of the summer circulation over the Qinghai-Xizang (Tibet) Plateau and its neighborhood. *Bull. Amer. Meteor. Soc.*, **62**, 14–19.

——, and Y.-X. Gao et al., 1979: *Meteorology of Qinghai-Xizang (Tibet) Plateau.* Science Press, Beijing, 278 pp. (in Chinese).

Yeh, T.-D., and Y.-X. Gao et al., 1979: *Meteorology of Qinghai-Xizang (Tibet) Plateau.* Science Press, Beijing, 278 pp. (in Chinese).

Yin, M. T., 1949: A synoptic-aerologic study of the onset of the summer monsoon over India and Burma. *J. Meteor.*, **6**, 393–400.

Zhou, X. and X. Hu, 1982: A brief analysis and numerical simulation of the Sichuan extraordinary heavy rainfall event in 1981. *Proc. First Sino-American Workshop on Mountain Meteorology*, Reiter, Zhu and Qian, Eds., Science Press, Beijing, 555–565.